SSRG International Journal of Electrical and Electronics Engineering
ISSN: 2348-8379/ https://doi.org/10.14445/23488379/IJEEE-V13I8P103

Volume 13 Issue 8, 22-34, August 2026

Original Article

Mechanical Parameter Estimation of an Induction Motor for a Digital Twin Using Coast-Down Data

Darjon Dhamo[1*], Aida Spahiu[1], Denis Panxhi[1], Nuri Rusta[2]

[1]*Automation Department, Polytechnic University of Tirana, Tirana, Albania.*
[2]*Electrical Engineering Department, Polytechnic University of Tirana, Tirana, Albania.*

[1*]*Corresponding Author : darjon.dhamo@upt.al*

Received: 06 April 2026 Revised: 24 May 2026 Accepted: 22 July 2026 Published: 25 August 2026

Abstract - *Accurate mechanical parameters are essential for developing Digital Twin (DT) models of Electric Drives (ED) that are both physically consistent and predictive across operating conditions. This paper presents an offline workflow for the mechanical parameter estimation and model validation of an Induction Motor (IM) drive for DT development. The experiments were performed on a laboratory setup in which an induction motor, supplied by a power converter, was mechanically coupled to an alternator through a belt–pulley transmission. Before parameter estimation, the measured voltage, current, and rotor speed signals are preprocessed, after which the coast-down interval is extracted from the full operating record for mechanical parameter identification. The mechanical parameters are then estimated through nonlinear least-squares fitting of the measured deceleration trajectories. The proposed procedure identifies the parameters that characterize the inertial and frictional behavior of the drive, enabling an accurate representation of the mechanical subsystem. A MATLAB/Simulink mechanical model is subsequently validated over separate time intervals and under operating conditions different from those used for estimation, so that any observed deviations can be attributed to model mismatch rather than to variations in parameter values with the operating point. Validation results show very good agreement between measured and simulated speed responses across multiple frequencies, with normalized root mean square error values of approximately (*$1.39 - 3.80\%$*) and (*$R^2 \geq 0.9964$*). These results demonstrate that the proposed workflow provides reliable and predictive mechanical parameters, forming a solid basis for future online adaptation and condition monitoring of induction motor drives.*

Keywords - *Coast-down experiments, Digital twins, Induction motors, Mechanical parameter estimation, Nonlinear least-squares estimation.*

1. Introduction

Induction motors remain among the most widely used electrical machines in industrial applications because of their robustness and low maintenance requirements for a broad range of operating conditions [2, 18]. As industrial systems increasingly move toward intelligent monitoring and predictive maintenance, the development of virtual representations of induction motor drives has become an important research direction [5, 6]. In this context, the Digital Twin (DT) concept has emerged as a promising framework for linking a physical asset with its computational counterpart in order to support analysis, diagnosis, and performance evaluation throughout the system lifecycle [9, 11]. The validity of such a framework depends strongly on the accuracy of the model parameters, as inaccurate parameter values can result in significant deviations between simulated and measured behaviour [14].

For induction motor drives, parameter estimation is commonly divided into two complementary parts: electrical parameter estimation and mechanical parameter estimation [3, 20]. The electrical subsystem is typically characterized by parameters such as stator resistance, rotor resistance, leakage inductances, and magnetizing inductance, which can be identified using standard tests or model-based estimation procedures [1, 16]. The electrical parameter estimation stage has been addressed in a separate study and is therefore not repeated here in detail. Instead, this work focuses on the mechanical subsystem, whose parameters are equally important for achieving a faithful dynamic representation of the drive, particularly during transients, acceleration and deceleration phases, and load-dependent operation [23, 24].

Even though proper initialization of parameters is necessary to develop accurate induction motor Digital Twins, much literature focuses on estimation of electrical parameters, control modelling, and general Digital Twin frameworks [21, 22]. Contrarily, the estimation of mechanical parameters, especially the identification of inertia and friction coefficients based on measurement data, is much less studied [3, 13]. Since these parameters cannot be found from a datasheet as they relate to the entire electromechanical drive, namely the shaft, coupling, transmissions, and load, applying nominal or approximate mechanical parameters results in discrepancies in the speed dynamics between the measurement and simulation, especially during deceleration and transient periods. This paper addresses this knowledge gap by proposing an experimental procedure for estimating mechanical parameters using the coast-down technique, which allows the integration of identified mechanical parameters into the offline calibration process of induction motor Digital Twin models.

Additionally, this paper proposes a systematic offline workflow for estimating the mechanical parameters of an induction motor by fitting a dynamic coast-down model to experimental speed data using Nonlinear Least Squares (NLS). The objective is to identify the inertia and friction parameters that minimize the mismatch between the measured rotor speed trajectory and the model-predicted deceleration response. Although coast-down-based mechanical parameter estimation has already been reported in previous studies [3, 20, 23, 24], the novelty of the present work lies in integrating this approach into a complete calibration workflow for induction motor Digital Twin development. In contrast to studies that mainly focus on electrical parameter estimation, control-oriented modelling, or general Digital Twin architectures [8, 10, 14, 21, 22], this work specifically addresses the mechanical subsystem and combines coast-down measurements, signal processing, dynamic model fitting, NLS estimation, and experimental validation against measured deceleration responses. Therefore, the contribution is not limited to obtaining numerical values of the mechanical parameters but also provides a practical initialization step for improving the fidelity of the virtual induction motor model used in Digital Twin applications.

Accordingly, the objectives of this paper are: (i) to formulate a mechanical model suitable for describing the coast-down dynamics of the induction motor; (ii) to estimate the unknown mechanical parameters through a nonlinear least-squares fitting procedure applied to experimental speed data; and (iii) to validate the estimated parameters by comparing measured and simulated deceleration responses. Through this study, the paper aims to provide a practical contribution to the offline calibration of induction motor models for digital twin development and related monitoring applications.

The remainder of this paper is organized as follows. Section II outlines the overall workflow adopted for mechanical parameter estimation from coast-down data. Section III describes the experimental platform, measurement and data-acquisition subsystems, signal-processing stage, mechanical model, and nonlinear least-squares estimation procedure, together with the validation methodology. Section IV presents the estimated parameters and discusses the corresponding estimation and validation results. Finally, Section V summarizes the main conclusions and highlights directions for future work.

2. Workflow for Mechanical Parameter Estimation

Figure 1 summarizes the mechanical parameter estimation workflow. It consists of six main steps: system implementation, measurement, data acquisition, signal processing, mechanical parameter estimation, and validation.

In Step 1, the experimental electric drive system is assembled and commissioned. The converter, induction motor, mechanical transmission, alternator, and battery are integrated into a laboratory test bench, and the correct operation of the system is verified before data collection. In Step 2, the required measurements are defined. For the mechanical subsystem, rotor speed is the primary measured variable used for parameter estimation. In addition, the measured voltage is used as input to the simulation model, while the current is also recorded as part of the synchronized measurement set. In Step 3, all signals are synchronously recorded and stored as time-series data using the DAQ system [5].

In Step 4, the acquired signals are processed. For the mechanical subsystem, this stage includes despiking, low-pass filtering, and selection of the coast-down interval from the complete operating record. The coast-down interval is chosen because, after supply removal, the electromagnetic torque becomes zero and the observed dynamics are dominated mainly by inertia and friction. This makes the coast-down regime more suitable for mechanical identification than powered operation, where electromagnetic torque and load disturbances are coupled [23, 24].

In Step 5, the mechanical parameters are estimated in the time domain using the MATLAB/Simulink induction-motor model and the measured coast-down speed trajectory [1, 3, 21, 23]. To improve the accuracy of parameter estimation, the coast-down record is divided into two consecutive intervals. In the high-speed interval, the dynamics are dominated mainly by inertia and viscous losses, so this region is used to estimate the inertia J and viscous friction coefficient B. In the low-speed interval, nonlinear friction effects become more evident; therefore, this region is used to estimate the Coulomb friction torque. T_C, breakaway torque T_{brk}, and breakaway angular speed ω_{brk}. The parameter values are obtained by Nonlinear Least-Squares (NLS) fitting, that is, by minimizing the difference between the measured speed $\omega(t)$ and the simulated speed. $\widehat{\omega}(t)$ over the corresponding interval.

In Step 6, the identified mechanical parameters are assigned to the simulation model and validated on coast-down data. Validation is performed by comparing the measured and simulated rotor-speed trajectories, analyzing the residuals, and computing summary fit metrics. In the full study, this validation strategy showed that a parameter set identified at one operating condition could reproduce the coast-down responses at other test frequencies with high accuracy. These results support the use of the calibrated mechanical subsystem as a reliable part of the baseline Digital Twin model [5, 21, 22].

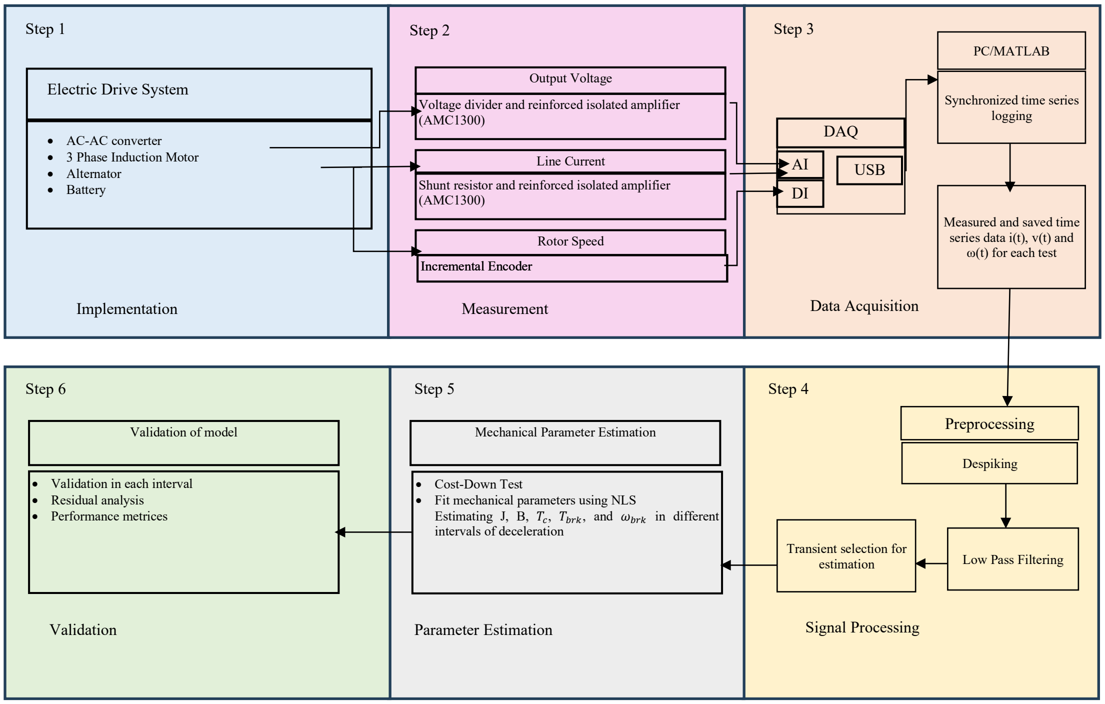

Fig. 1 Offline parameter estimation workflow

3. Materials and Methods

3.1. System Implementation

The proposed mechanical parameter estimation procedure was validated on the laboratory induction motor drive platform developed for Digital Twin calibration. The setup includes an induction motor supplied by a Variable Frequency Drive (VFD) and mechanically coupled to a loading unit through a belt--pulley mechanism, enabling repeatable transient tests under controlled laboratory conditions. In the present study, the emphasis is placed on the mechanical subsystem, since the measured speed of the rotor is used to identify the inertia and friction parameters of the corresponding virtual model. The experimental arrangement is illustrated in Figure 2, and the main specifications of the drive components are reported in Table 1.

The present work focuses specifically on coast-down dynamics and validation using speed measurements.

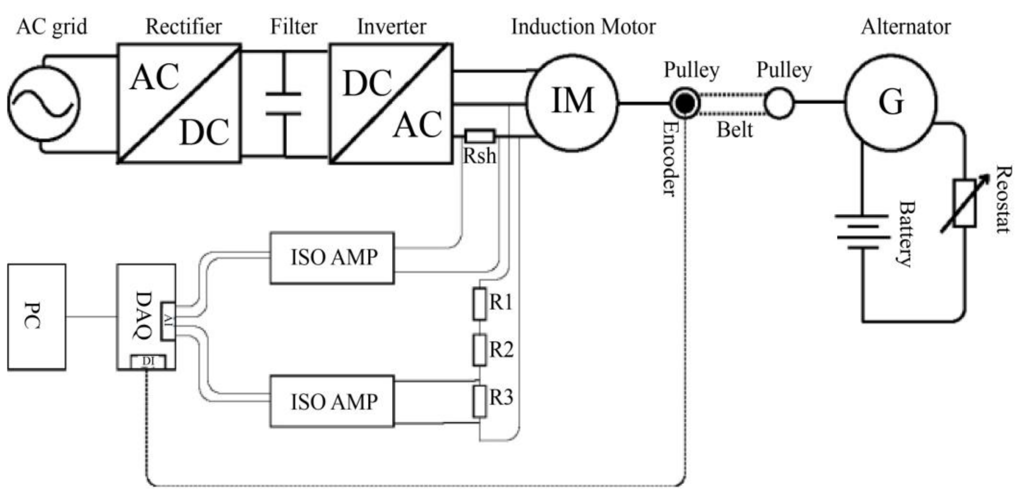

Fig. 2 Diagram of the experimental electric drive test bench and its measurement configuration

Table 1. Technical specifications of the IM electric drive components

Technical Specification	Value
VFD (FR-D720S-014SC-EC)	
Rated input voltage (single-phase)	200-240 V AC
Permissible input voltage range	170-264 V AC
Rated motor capacity (ND)	0.2 kW
Rated output current (ND)	1.4 A
Output frequency range	0.2-400 Hz
Induction Motor (IM)	
Rated power	130 W
Rated voltage (Y/Δ)	380/220 V
Rated current (Y/Δ)	0.38/0.66 A
Rated frequency	50 Hz
Rated speed	2900 rpm
Alternator (G)	
Nominal output voltage	14 V
Rated output current	95 A
Part number	7700 437 090
Battery	
Nominal voltage	12 V
Capacity	62 Ah
Model	W62 L2D
Rheostat	
Resistance	7.5 Ω
Current	10 A

3.2. Measurements

Table 2 summarizes the main specifications of the measurement subsystem. Current is measured using a shunt resistor connected in series, while voltage is measured through a voltage divider circuit adapted to the inverter output level. The resulting electrical signals are conditioned and electrically isolated before being sent to the data-acquisition step. This improves measurement safety and reduces unwanted coupling effects between the power and instrumentation circuits. For the mechanical subsystem, rotor speed is measured by an incremental encoder mounted on the motor shaft. These signals provide the experimental basis for parameter estimation and model validation.

Table 2. Measurement components and specifications

Technical Specification	Value
Shunt Resistor	
Part	Vishay
Resistance	0.1 Ω
Power rating	3 W
Tolerance	±1%
Technology/package	Wirewound, axial leaded
Voltage Divider	
Upper divider resistor	R1 = 2.2 MΩ, 1/4 W, ±5%
Middle divider resistor	R2 = 1 MΩ, 1/4 W, ±5%
Bottom divider resistor	R3 = 1 kΩ, 1/4 W, ±5%
Isolated Amplifier	
Device	TI AMC1300
Input range (peak)	±250 mV
Gain	8.2 (fixed)
Isolation rating	Reinforced; 5000 VRMS for 1 min.
Output type	Differential
Incremental Encoder	
Model	Autonics E40S6-1000-3-T-24

Supply voltage	12-24 VDC
Resolution	1000 pulses/rev
Shaft diameter	6 mm
Cable length/protection	2 m; IP50

3.3. Data Acquisition

Voltage, current, and rotor-speed signals are sampled using an NI USB-6009 data-acquisition device connected to a PC, where they are logged and processed in MATLAB. The conditioned voltage and current signals are sampled through differential analog inputs, whereas the encoder signal is used to reconstruct the rotor speed.

The recorded channels are organized as synchronized time-series data and then converted into physical quantities using appropriate scaling coefficients. In the present study, these measurements are employed for parameter estimation and model validation, focusing in particular on the measured behaviour of the mechanical subsystem. The principal specifications of the NI USB-6009 are listed in Table 3, while representative acquired waveforms are presented in Figure 3.

Table 3. Principal specifications of the NI USB-6009

Specification	**Value**
NI USB-6009	
AI channels (SE/DIFF)	8 / 4
AI resolution (SE/DIFF)	13 / 14 bit
Max AI sample rate (agg.)	48 kS/s
AI input range	±10 V (SE), up to ±20 V (DIFF)
Digital I/O	12 lines
Counter/timer	1 × 32-bit
Interface	USB (bus-powered)
Configuration used in this work	
AI mode/channels	DIFF / 2 (V, I)
DI lines	Encoder A, B (Z optional)
Sampling rate	20 kS/s per AI
Software	MATLAB

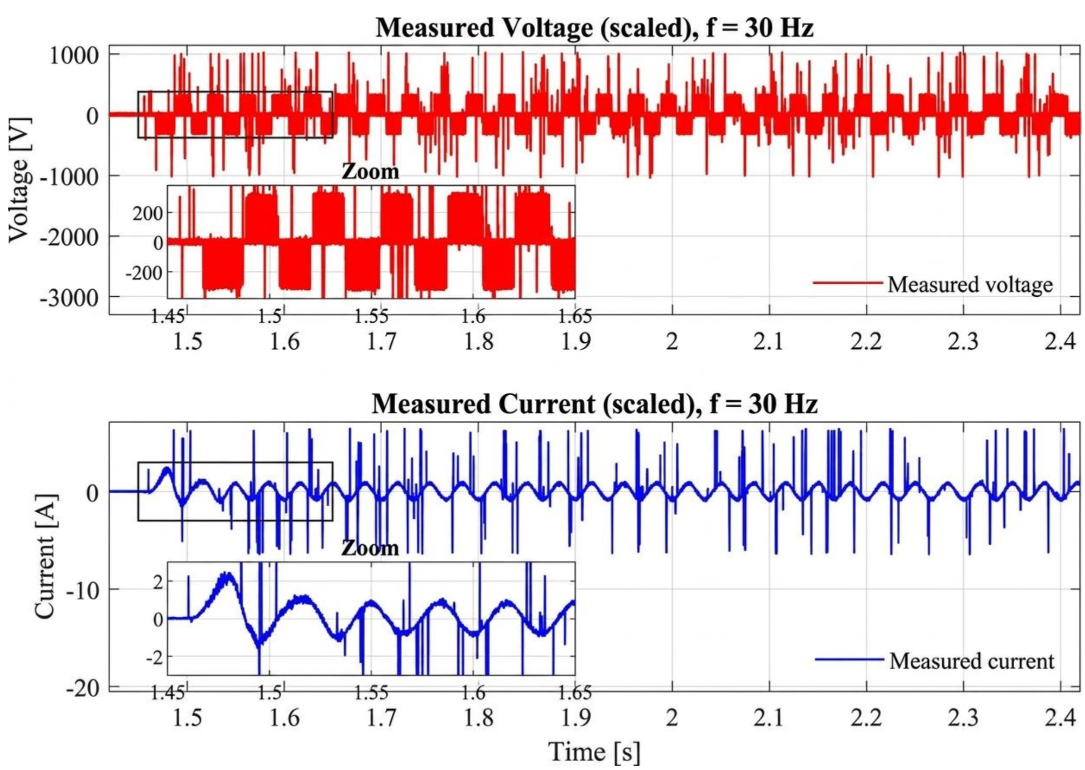

Fig. 3 Measured DAQ signals

3.4. Signal Processing

In this phase, signal-processing techniques are applied to the voltage, current, and speed measurements for mechanical parameter estimation during the coast-down transient. A despike and filtering pipeline for mechanical parameter estimation is employed [3, 13].

3.4.1. Despike

When the variable speed drive starts generating the three-phase output using PWM, the fast switching edges (dv/dt) create high-frequency components that couple into the voltage and current measurements. These appear as thin spikes overlaid on the waveforms, which are not representative of the actual motor physics. Therefore, the measurement signals were filtered. The method used for despiking is described in the following paragraph.

The term $x[n]$ in (Equation 1) refers to the measured channel (current or voltage) sampled at $f_s = 20\ kHz$ with $n = 0, 1, \ldots, n-1$ and $t_n = n/f_s$. To remove spikes, a median-filtered version of the measured signal, computed over a short sliding window, is used as a reference. Specifically, a window of $T_\omega = 0.1$ was used, corresponding to $W = round(T_\omega \cdot f) \approx 2$ samples. The median-filtered reference is denoted by $x_{med}[n]$, and the absolute deviation from this reference is as follows:

$$d[n] = |x[n] - x_{med}[n]| \tag{1}$$

A global dispersion estimate was subsequently obtained from the median of the deviations:

$$\hat{\sigma} = 1.4826\, median(d[n]) \tag{2}$$

A sample was classified as a spike if its deviation exceeded a multiple of this robust scale:

$$d[n] > k_\sigma \hat{\sigma} \tag{3}$$

Detected spikes were then replaced with the corresponding values of the median reference as described in Equation (4):

$$x_{ds}[n] = \begin{cases} x_{med}[n] & if\ n\ is\ classified\ as\ a\ spike \\ x[n] & otherwise \end{cases} \tag{4}$$

This produces the despiked signal. $x_{ds}[n]$, visualized in Figure 4.

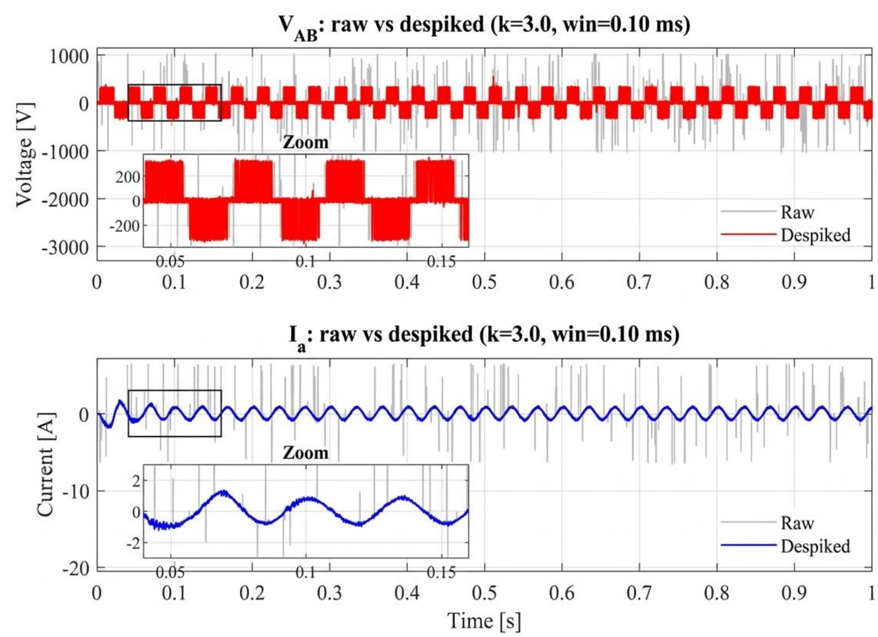

Fig. 4 Real measurement versus despiked signals

After despiking, the signal $x_{ds}[n]$ is smoothed by a fourth-order Butterworth low-pass filter with a cutoff frequency f_c. Figure 5 visualizes an example with $f_c = 80Hz$ for a 30 Hz fundamental component. The digital Infinite Impulse Response (IIR) filter with coefficients. $\{b_k\}$ and $\{a_k\}$ ($a_0 = 1$) is defined as:

$$y[n] = \sum_{k=0}^{M} b_k x_{ds}[n-k] - \sum_{k=1}^{p} a_k y[n-k] \tag{5}$$

Zero-phase filtering is obtained by applying the same IIR filter forward and then backward in time. Let $\mathcal{H}\{\cdot\}$ denote the filtering operation defined above, and let $\mathcal{R}\{\cdot\}$ denote the time-reversal operator:

$$(\mathcal{R}x)[n] = x[N-1-n] \tag{6}$$

The zero-phase filtered output is:

$$x_f = \mathcal{R}\{\mathcal{H}(\mathcal{R}\{\mathcal{H}(x_{ds})\})\} \tag{7}$$

Neglecting boundary transients, the resulting transfer function becomes:

$$H_{ff}(z) = H(z)H(z^{-1}) \tag{8}$$

and, consequently, on the unit circle:

$$X_f(e^{j\omega}) = \left|H(e^{j\omega})\right|^2 X_{ds}(e^{j\omega}) \tag{9}$$

which removes the phase shift.

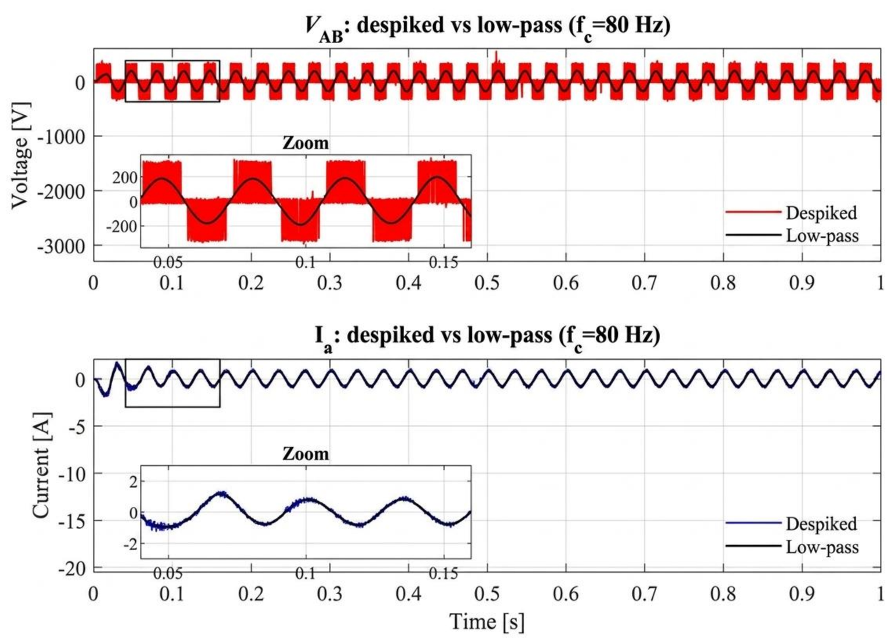

Fig. 5 Despiked signals versus low-pass filtered signals

3.5. Mechanical Parameter Estimation

The electrical parameters of the IM model $(R_s, R_r', L_\sigma, L_m)$ were obtained from prior experimental parameter identification of the same induction motor. These parameters were not re-estimated in the present work and were therefore treated as fixed values in the model implementation.

In the model implementation, the total leakage inductance was split equally as $L_{s\sigma} = L'_{\sigma s} = L_\sigma/2$. Consequently, only the mechanical parameters were estimated in the present study. Electrical parameter values are reported in Table 4.

Table 4. Estimated induction motor electrical parameters used in the model

Symbol	Value	Unit
R_s	60.5	Ω
R_r'	42.2	Ω
L_σ	0.66	H
L_m	1.73	H

In this work, these parameters were estimated from the coast-down transient at a VFD operating frequency of 40 Hz. The interval is not taken immediately after disconnection because the residual rotor-flux transient induces a stator back-EMF (Figure 6) and introduces additional magnetic losses. This transient decays over the time constant $\tau_0 = L_{rr}/R_r$; therefore, this interval was discarded, and the mechanical estimation started only after τ_0.

Moreover, the mechanical parameter estimation was performed with the IM connected in star to avoid delta circulating currents, which can produce an additional braking torque and bias the estimated parameters. This experiment was well-suited for mechanical parameter estimation because the dominant dynamics are governed by inertia and friction [3, 13].

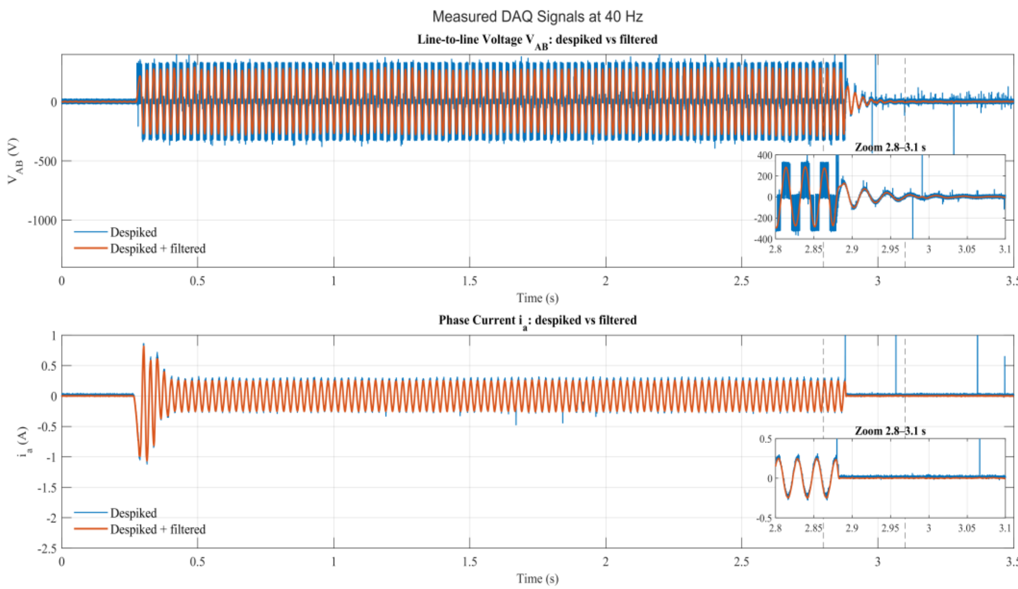

Fig. 6 Signals of voltage and current at a VFD operating frequency of 40 Hz

Mechanical parameter estimation was carried out using the induction motor dynamic model formulated in the synchronous dq reference frame ([25, 26]) and implemented in MATLAB/Simulink.

With $\dot{\psi} = d\psi/dt$ denoting the time derivative of the flux linkage and $\omega_{sl} = \omega_e - \omega_r$ denoting the slip frequency, the voltage equations are expressed as:

$$v_{ds} = R_s i_{ds} + \dot{\psi}_{ds} - \omega_e \psi_{qs} \quad (10)$$

$$v_{qs} = R_s i_{qs} + \dot{\psi}_{qs} - \omega_e \psi_{ds} \quad (11)$$

$$0 = R'_r i_{dr} + \dot{\psi}_{dr} - \omega_{sl} \psi_{qr} \quad (12)$$

$$0 = R'_r i_{qr} + \dot{\psi}_{qr} - \omega_{sl} \psi_{dr} \quad (13)$$

The flux linkages are described by:

$$\psi_{ds} = L_{ss} i_{ds} + L_m i_{dr}, \;\; \psi_{qs} = L_{ss} i_{qs} + L_m i_{qr} \quad (14)$$

$$\psi_{dr} = L_m i_{ds} + L_{rr} i_{dr}, \psi_{qr} = L_m i_{qs} + L_{rr} i_{qr} \quad (15)$$

where $L_{ss} = L_{\sigma s} + L_m$ and $L_{rr} = L_{\sigma r} + L_m$ are the stator and rotor self-inductances. The electromagnetic torque is computed from Equation (16):

$$T_e = \frac{3}{2} p\left(\psi_{ds} i_{qs} - \psi_{qs} i_{ds}\right) \quad (16)$$

with p denoting the number of pole pairs.

The moment balance of the induction motor is formulated in Equation (17):

$$J\dot{\omega}_m = T_e - T_L - T_f(\omega_m) \quad (17)$$

where J is the equivalent inertia referred to the motor shaft, T_L is the load torque, and $T_f(\omega_m)$ is the friction torque. The friction torque is written as a sum of breakaway, Coulomb, and viscous components:

$$T_f(\omega_m) = \sqrt{2e}(T_{brk} - T_C) exp\left[-\left(\frac{\omega_m}{\omega_{st}}\right)^2\right]\left(\frac{\omega_m}{\omega_{st}}\right) + T_C tanh\left(\frac{\omega_m}{\omega_{Coul}}\right) + B\omega_m \quad (18)$$

The velocity thresholds are defined as follows:

$$\omega_{st} = \omega_{brk}\sqrt{2}, \;\; \omega_{Coul} = \frac{\omega_{brk}}{10} \quad (19)$$

The first term captures the Stribeck effect. The second term models Coulomb friction with a smooth sign transition controlled by ω_{Coul}. The last term represents viscous friction proportional to speed.

3.5.1. Nonlinear Least-Squares Estimator

The nonlinear least-squares method is used in the literature for the estimation of IM parameters. Here, the nonlinear least-squares method was used for mechanical parameter estimation. Mechanical parameters are estimated from the measured coast-down speed. $\omega_m^{meas}(t_k)$ by matching the simulated speed $\omega_m^{sim}(t_k;\theta)$ over the coast-down interval. The estimation intervals were selected to isolate the dominant physical effects in each speed range. In the high- and medium-speed region (1600-750 rpm), the coast-down was governed by the inertial term $J\dot{\omega}$ Moreover, the viscous friction term $B\omega$, while dry-friction effects were comparatively small. In the lower-speed region (750-300 rpm), dry-friction contributions became comparable to viscous losses, so the coefficients. T_C and T_{brk} could be estimated more reliably from the shape of the coast-down curve. Finally, in the very low-speed range (300-80 rpm), friction becomes strongly speed dependent and cannot be adequately captured by parameters estimated at higher speeds. Therefore, ω_{brk} was fitted in this interval to represent the final-stage coast-down dynamics.

The estimated parameter vector is introduced in Equation (20):

$$\theta = [J, B, T_c, T_{brk}, \omega_{brk}]^T \quad (20)$$

The nonlinear least-squares estimation is formulated in Equation (21):

$$\dot{\theta} = arg\min_{\theta} \sum_{k=1}^{N} \left(\omega_m^{meas}(t_k) - \omega_m^{sim}(t_k;\theta)\right)^2 \quad (21)$$

The resulting parameters were retained for the final DT model and were further used in subsequent validation runs.

3.6. Validation

The validation of the mechanical subsystem was based on coast-down experiments. The mechanical parameters were identified from the transient recorded at a VFD operating frequency of $40Hz$ and subsequently validated using coast-down responses obtained at $45Hz, 50Hz,$ and $55Hz$. In each validation test, the simulated rotor-speed trajectory was compared with the corresponding measured speed response. Model performance was evaluated by means of residual analysis together with quantitative metrics such as RMSE, NRMSE, and R^2.

In this way, the validation examined the capability of the estimated mechanical parameters to represent the drive dynamics beyond the operating condition used for parameter identification.

4. Results and Discussion

4.1. Mechanical Parameter Estimation

Experimental results related to the mechanical parameter estimation are visualized in Figures 7 and 8, and the estimated parameters are shown in Table 5. The primary curve plotted in Figure 7 illustrates the measured and estimated values of the speed versus time during the coast-down test conducted at 40 Hz, whereas the small inset demonstrates the window used to fit the parameters of the machine.

This particular window corresponds to the region of the transient that gives the best information concerning the inertia and friction forces dominating the system. Results in Figure 7 prove that the estimated parameters provide a good reproduction of the system dynamics.

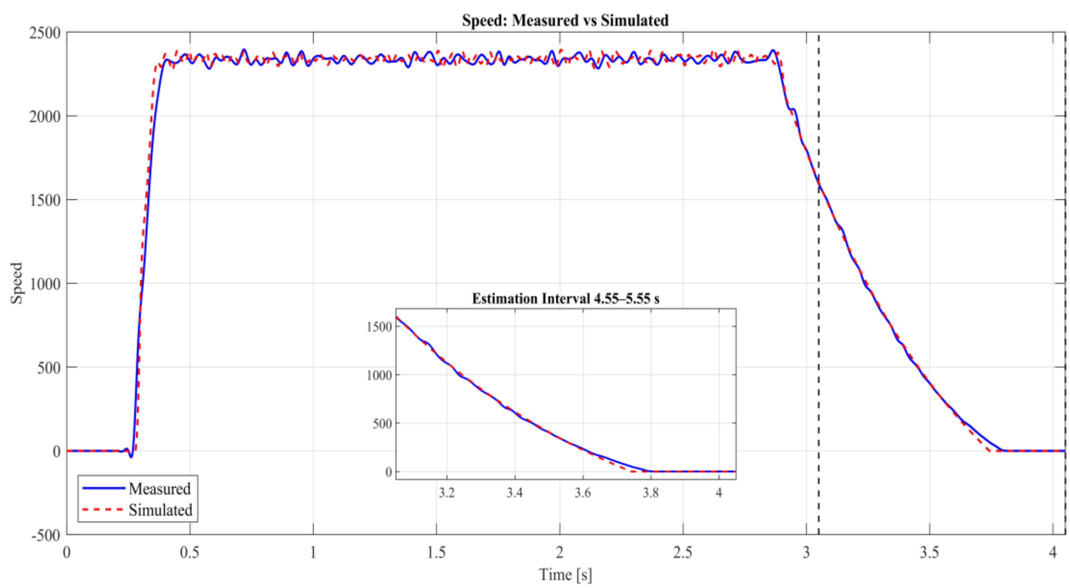

Fig. 7 Coast-Down speed at $40Hz$ and selected estimation window (measured versus simulated)

A consistent set of mechanical parameters was identified from the $40Hz$ coast-down test, as summarized in Table 5. The estimated inertia is small, which is expected for a 130 W induction motor. The viscous friction coefficient is also low, consistent with the gradual coast-down observed over most of the speed range. As the speed decreases, the influence of dry friction becomes more pronounced. The estimated breakaway torque is slightly higher than the Coulomb friction torque ($T_{brk} > T_C$), indicating a modest Stribeck-type reduction from breakaway friction to steady sliding friction. Finally, the breakaway speed parameter ω_{brk} governs the smooth transition to stiction near zero speed and improves the model's capability to reproduce the final stage of the coast-down. Overall, both the magnitudes and the ordering of the estimated parameters are consistent with the expected physics of the deceleration process and provide a stable mechanical subsystem for the calibrated DT.

Table 5. Estimated mechanical parameters from the Coast-Down experiment at $40Hz$

Symbol	Value	Unit
J	8.7499×10^{-5}	$kg \cdot m^2$
B	1.0791×10^{-4}	$N \cdot m \cdot s/rad$
T_C	0.012998	$N \cdot m$
T_{brk}	0.014236	$N \cdot m$
ω_{brk}	0.02	rad/s

Figure 8 compares the measured and simulated speed trajectories over the estimation interval and also presents the corresponding residual signal. The simulated response closely follows the measured coast-down profile, confirming that the estimated parameter set captures the dominant slope of the deceleration.

The residual remains small relative to the overall speed range and exhibits only limited deviations near the end of the interval. This behaviour is likely associated with the reduced accuracy of encoder-based speed estimation at low speed, together with the greater difficulty of reproducing strongly nonlinear friction effects in this region.

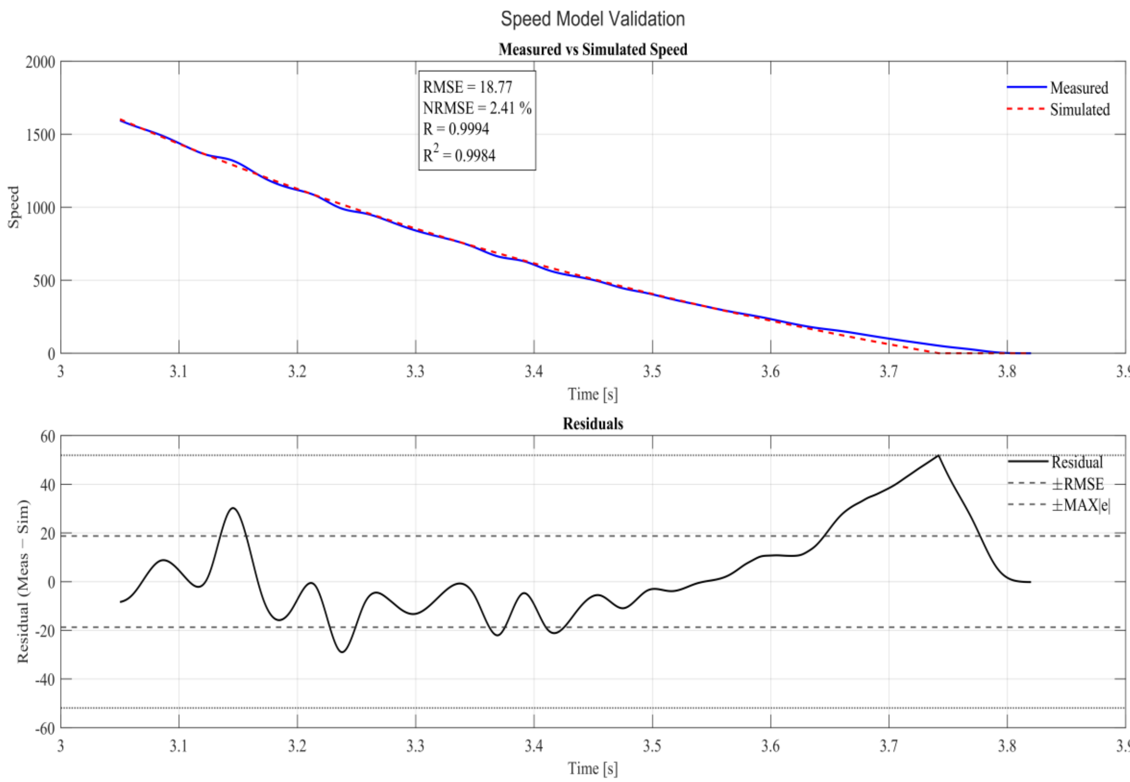

Fig. 8 Mechanical model fit on the $40Hz$ estimation interval: measured versus simulated speed and residual signal

4.2. Mechanical Model Validation

Figure 9 presents the mechanical validation at $50Hz$ by comparing the measured coast-down speed with the simulated speed obtained using the parameter set identified at $40Hz$, namely J, B, T_C, T_{brk}, and ω_{brk}. The measured and simulated speed profiles overlap closely over the full interval, indicating that the estimated inertia and friction parameters capture the dominant coast-down dynamics at this operating point.

The residual, defined as the difference between the measured and simulated speed, remains bounded near zero, with a slight drift in the final portion of the record as the machine approaches very low speed. This behaviour is consistent with the estimation run at $40Hz$ and can be attributed to the reduced accuracy of encoder-based speed estimation near zero speed, together with the increasing influence of nonlinear friction effects in this region.

Quantitative validation results are summarized in Table 6, where the same parameter set identified at $40Hz$ is tested on coast-down experiments at $45Hz$, $50Hz$, and $55Hz$. The model achieves excellent agreement at 50Hz, with $NRMSE = 1.39\%$ and $R^2 = 0.9995$. At $45Hz$ and $55Hz$, the mismatch increases slightly, but it remains small relative to the overall speed range. The largest deviation is observed at $55Hz$, where $NRMSE = 3.80\%$ and $R^2 = 0.9964$, which still indicates strong agreement between model and experiment. These results confirm that the identified mechanical parameters remain predictive when applied to operating conditions different from those used for estimation.

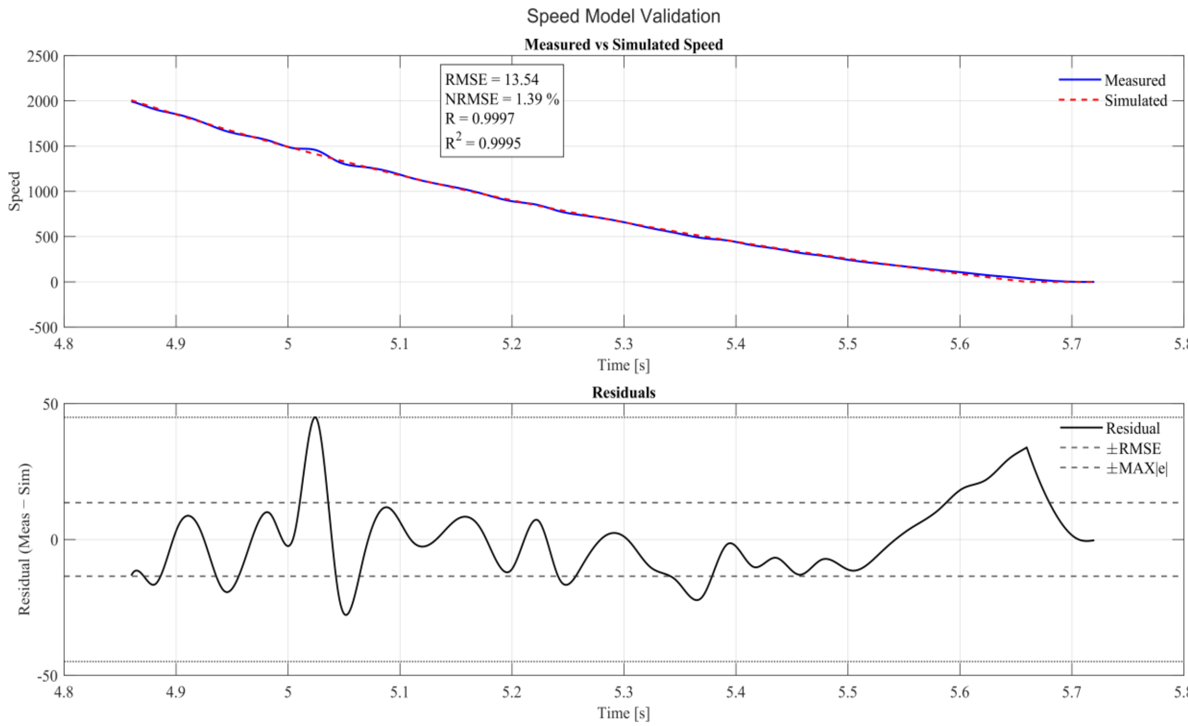

Fig. 9 Mechanical validation at $50Hz$: measured versus simulated speed and residual signal obtained using the parameter set identified at $40Hz$

Table 6. Mechanical parameter validation

f (Hz)	RMSE (rpm)	NRMSE (%)	R^2
45	19.33	2.26	0.9987
50	13.54	1.39	0.9995
55	39.55	3.80	0.9964

Overall, the validation results justify the use of the estimated mechanical parameters in the calibrated mechanical subsystem of the DT. They show that the identified parameter set not only reproduces the estimation case but also maintains high predictive accuracy over additional coast-down experiments performed at different operating frequencies.

5. Conclusion and Future Work

This paper addressed the offline calibration of the mechanical subsystem of an induction motor digital twin using coast-down experiments and nonlinear least-squares estimation. The study focused specifically on the identification of the inertia and friction parameters after the electrical subsystem had been treated separately. To this end, a workflow was developed that combines synchronized measurement acquisition, processing of the coast-down record, interval-based identification of the dominant mechanical effects, and model validation on operating conditions different from those used for estimation. The estimated parameter set was physically consistent and enabled the MATLAB/Simulink model to reproduce the measured deceleration behaviour with high accuracy. Compared to traditional methods for identifying the coast-down parameters using graphical, linear, and single condition approaches described by different authors, the suggested technique is more reliable because the dynamic coast-down model is fitted directly to the experimentally observed speed data, and the identified parameters are verified in an independent manner using different supply frequencies. The higher accuracy of the response matching may be justified by three main factors: (i) a proper selection of the estimation interval corresponding to the most relevant phase of the coast-down response; (ii) the application of the nonlinear least-squares estimation procedure that eliminates discrepancies across the entire fitting interval instead of the approximation based only on local slopes; and (iii) the verification of the identified parameters for different supply frequencies. In particular, the parameters identified from the 40Hz coast-down experiment remained predictive when applied to independent validation tests at 45, 50, and 55Hz, producing NRMSE values between 1.39% and 3.80% and coefficients of determination not lower than $R^2 = 0.9964$. These results show that the proposed procedure provides a reliable offline calibration stage for the mechanical part of the digital twin and establishes a consistent basis for subsequent monitoring and simulation tasks.

5.1. Future Work

Future work will extend the present mechanical calibration stage toward a more complete digitally updated twin based on experimental measurements. One direction is the integration of the validated mechanical subsystem with online updating strategies capable of tracking changes in inertia and friction under varying loading conditions. Another direction is the use of the calibrated model for higher-level applications such as condition monitoring, fault detection, and predictive maintenance of the electric drive. In addition, more advanced friction representations and adaptive estimators may be investigated in order to improve the model accuracy in the low-speed region, where nonlinear friction effects and encoder resolution limitations become more significant.

Conflicts of Interest

The authors declare that there is no conflict of interest regarding the publication of this paper.

Funding Statement

This research received no external funding.

References

[1] Kaiyu Wang et al., “A Nonlinear Least-Squares Approach for Identification of the Induction Motor Parameters,” *IEEE Transactions on Automatic Control*, vol. 50, no. 10, pp. 1622-1628, 2005. [CrossRef] [Google Scholar] [Publisher Link]

[2] D. Lindenmeyer et al., “An Induction Motor Parameter Estimation Method,” *International Journal of Electrical Power and Energy Systems*, vol. 23, no. 4, pp. 251-262, 2001. [CrossRef] [Google Scholar] [Publisher Link]

[3] Mohsen Soori, Behrooz Arezoo, and Roza Dastres, “Digital Twin for Smart Manufacturing: A Review,” *Sustainable Manufacturing and Service Economics*, vol. 2, pp. 1-15, 2023. [CrossRef] [Google Scholar] [Publisher Link]

[4] Mohsen Ebadpour et al., “Digital Twin Model of Electric Drives Empowered by EKF,” *Sensors*, vol. 23, no. 4, pp. 1-21, 2023. [CrossRef] [Google Scholar] [Publisher Link]

[5] Jhennifer F. Dos Santos et al., “Digital Twin-based Monitoring System of Induction Motors using IoT Sensors and Thermo-Magnetic Finite Element Analysis,” *IEEE Access*, vol. 11, pp. 1682-1693, 2023. [CrossRef] [Google Scholar] [Publisher Link]

[6] Weiming Yin et al., “Digital Twin-Driven Condition Monitoring System for Traditional Complex Machinery in Service,” *Machines*, vol. 13, no. 6, pp. 1-21, 2025. [CrossRef] [Google Scholar] [Publisher Link]

[7] Fei Tao et al., “Digital Twin-Driven Product Design, Manufacturing and Service with Big Data,” *International Journal of Advanced Manufacturing Technology*, vol. 94, no. 9, pp. 3563-3576, 2017. [CrossRef] [Google Scholar] [Publisher Link]

[8] Yuqian Lu et al., “Digital Twin-Driven Smart Manufacturing: Connotation, Reference Model, Applications and Research Issues,” *Robotics and Computer-Integrated Manufacturing*, vol. 61, pp. 1-14, 2020. [CrossRef] [Google Scholar] [Publisher Link]

[9] Ke Zhang et al., “Digital Twin-Enabled Predictive Thermal Modeling for Stator Temperature Monitoring in Induction Motors,” *Electronics*, vol. 14, no. 14, pp. 1-19, 2025. [CrossRef] [Google Scholar] [Publisher Link]

[10] Michael Grieves, and John Vickers, “Digital Twin: Mitigating Unpredictable, Undesirable Emergent Behavior in Complex Systems,” *Transdisciplinary Perspectives on Complex Systems*, pp. 85-113, 2016. [CrossRef] [Google Scholar] [Publisher Link]

[11] Guillaume Pronost et al., “Digital Twins along the Product Lifecycle: A Systematic Literature Review of Applications in Manufacturing,” *Digital Twin*, vol. 1, no. 2, pp. 1-31, 2024. [CrossRef] [Google Scholar] [Publisher Link]

[12] Diptarshi Bhowmick, and Suparna Kar Chowdhury, “Estimation of Induction Motor Equivalent Circuit Parameters and Losses from Transient Measurement,” *ISA Transactions*, vol. 157, pp. 573-590, 2025. [CrossRef] [Google Scholar] [Publisher Link]

[13] Fatma Zohra Aboubi et al., “Experimental Identification of a Coupled-Circuit Model for the Digital Twin of a Wound-Rotor Induction Machine,” *Energies*, vol. 17, no. 8, pp. 1-25, 2024. [CrossRef] [Google Scholar] [Publisher Link]

[14] Zhiwei Gao, Anand Paul, and Xiaokang Wang, “Guest Editorial: Digital Twinning: Integrating AI-ML and Big Data Analytics for Virtual Representation,” *IEEE Transactions on Industrial Informatics*, vol. 18, no. 2, pp. 1355-1358, 2022. [CrossRef] [Google Scholar] [Publisher Link]

[15] Tomas Kostal, and Pavel Kobrle, “Induction Machine On-Line Parameter Identification for Resource-Constrained Microcontrollers based on Steady-State Voltage Model,” *Electronics*, vol. 10, no. 16, pp. 1-19, 2021. [CrossRef] [Google Scholar] [Publisher Link]

[16] Azad M. Madni, Carla C. Madni, and Scott D. Lucero, “Leveraging Digital Twin Technology in Model-based Systems Engineering,” *Systems*, vol. 7, no. 1, pp. 1-13, 2019. [CrossRef] [Google Scholar] [Publisher Link]

[17] V.P. Sakthivel, R. Bhuvaneswari, and S. Subramanian, “Multi-Objective Parameter Estimation of Induction Motor using Particle Swarm Optimization,” *Engineering Applications of Artificial Intelligence*, vol. 23, no. 3, pp. 302-312, 2010. [CrossRef] [Google Scholar] [Publisher Link]

[18] Chiara Cimino, Elisa Negri, and Luca Fumagalli, “Review of Digital Twin Applications in Manufacturing,” *Computers in Industry*, vol. 113, pp. 1-15, 2019. [CrossRef] [Google Scholar] [Publisher Link]

[19] Gusztáv Áron Sziki, Attila Szántó, and Éva Ádámkó, “Review of Methods for Determining the Moment of Inertia and Friction Torque of Electric Motors,” *Acta Polytechnica Hungarica*, vol. 21, no. 4, pp. 203-218, 2024. [CrossRef] [Google Scholar] [Publisher Link]

[20] Adamou Amadou Adamou et al., “Squirrel Cage Induction Motors Accurate Modelling for Digital Twin Applications,” *Modelling*, vol. 5, no. 4, pp. 1582-1600, 2024. [CrossRef] [Google Scholar] [Publisher Link]

[21] R. Raja Singh et al., “Building a Digital Twin Powered Intelligent Predictive Maintenance System for Industrial AC Machines,” *Machines*, vol. 11, no. 8, pp. 1-20, 2023. [CrossRef] [Google Scholar] [Publisher Link]

[22] V.S.S. Pavan Kumar Hari, Avanish Tripathi, and G. Narayanan, “Experimental Determination of Mechanical Parameters in Sensorless Vector-Controlled Induction Motor Drive,” *Sādhanā*, vol. 42, no. 8, pp. 1285-1297, 2017. [CrossRef] [Google Scholar] [Publisher Link]

[23] Attila Szántó et al., "Simultaneous Measurement of the Moment of Inertia and Braking Torque of Electric Motors Applying Additional Inertia," *Measurement*, vol. 204, pp. 1-7, 2022. [CrossRef] [Google Scholar] [Publisher Link]

[24] J.O. Ojo, A. Consoli, and T.A. Lipo, "An Improved Model of Saturated Induction Machines," *IEEE Transactions on Industry Applications*, vol. 26, no. 2, pp. 212-221, 1990. [CrossRef] [Google Scholar] [Publisher Link]

[25] Sergey Edward Lyshevski, *Electromechanical Systems, Electric Machines, and Applied Mechatronics*, 1st ed., Boca Raton, CRC Press, 2018. [CrossRef] [Google Scholar] [Publisher Link]

[26] Prabha S. Kundur, *Power System Stability and Control*, 3rd ed., Boca Raton, CRC Press, 2016. [Google Scholar]